PRELIMINARY DEVELOPMENT OF A 4D ANATOMICAL MODEL FOR MONTE CARLO SIMULATIONS

X. George Xu
Nuclear Engineering and Engineering Physics Program
Rensselaer Polytechnic Institute
Troy, NY 12180, USA
xug2@rpi.edu

Chengyu Shi
Department of Radiation Oncology
University of Arkansas for Medical Sciences
Little Rock, AR 72205, USA
cshi@uams.edu

ABSTRACT

Existing anatomical models are mostly representative of three-dimensional (3D) standing individuals, based on either stylized surface equations (the so-called MIRD models) or tomographic images (the so-called voxel models). This paper presents a method to develop a 4D anatomical model using the existing 3D VIP-Man model, the Non-Uniform Rational B-Splines (NURBS) method and clinically obtained respiratory motion data. A lesion in the left lung is simulated to study how the organ motions may affect dose to the lesion. The procedure to simulate the 4D VIP-Man models for Monte Carlo simulations using EGS code is described. This preliminary study demonstrates that the motion of the organs can be modeled in the Monte Carlo code for more accurate dose calculations. Although the study was based on the VIP-Man images, the method can be extended to patient specific models constructed, for example, from multi-slice CT images.

Key words: 4D, Monte Carlo, Anatomical Model, EGS4.

1 INTRODUCTION

Radiation doses to a person (a patient or a worker) are often calculated using the Monte Carlo methods and human body models. Existing 3-dimensional (3D) whole-body anatomical models are mostly representative of individuals who are in a standing position, without considering the motion of the heart and limbs, or changes of the body posture. Over the years, computational patient models have evolved into two types: 1) Equation-based stylized models, where organs are delineated by a combination of simple surface equations, and 2) Image-based tomographic models, in which organs are defined from segmented and labeled volume elements (voxels) from tomographic images of real individuals.

1.1 Stylized models

Stylized anatomical models were originally developed for the Medical Internal Radiation Dosimetry (MIRD) Committee of the Society of Nuclear Medicine (SNM) in 1970's [1]. Fig. 1a illustrates the stylized adult. There are only three media with distinct densities: bone, soft tissue, and lung. These models were analytically defined in three principal sections: an elliptical cylinder resenting the arm, torso, and hips; a truncated elliptical cone representing the legs and feet; and an elliptical cylinder representing the head and neck. Fig. 1b shows the internal organs and tissues and Fig. 1c shows the stomach and gastrointestinal (GI) tract.

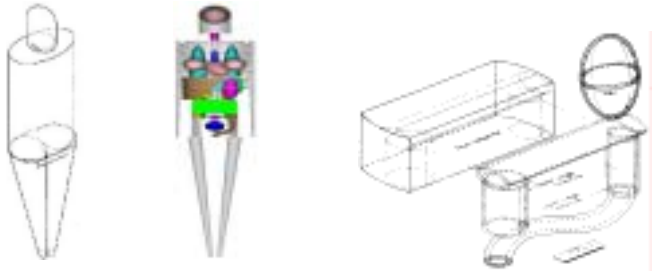

(a) (b) (c)

Figure 1. Stylized adult male models showing (a) exterior view of the adult male, (b) skeleton and internal organs of the adult male/female, (c) surface equations representing stomach and GI tract.

The stylized mathematical descriptions of the organs were formulated based on descriptive and schematic materials from general anatomy references. The goal of this approach was to make the equations simple, thus minimizing computing time [2]. For thirty years, these simplified models have been used as the de facto "standard" representations of the "Reference Man" [3] for radiation protection, nuclear medicine, and medical imaging [4-6]. The problem with the existing stylized models is that the shapes are not realistic when compared to a real person.

1.2 Tomographic Models

In the past decade, a new class of computational models has emerged with the advent of 3D tomographic imaging. These models contain large arrays of voxels that are identified in terms of tissue type (soft tissue, hard bone, air, etc) and unique organ identification (lungs, liver, skin, etc). Tomographic images reveal patient internal structures accurately, but time-consuming segmentation and classification are necessary to implement the models for radiation transport calculations in a Monte Carlo code. To date, a number of major studies have reported whole-body tomographic models [7].

In 2000, Xu et al. from Rensselaer reported the development of an adult male patient model, called VIP-Man [8]. This model was based on anatomical color images of the Visible Man from the Visible Human Project (VHP) [9, 10]. The original image resolution of the Visible Man is 0.33-mm x 0.33-mm and the slice thickness is 1 mm which allowed for small and

radiosensitive structures to be identified and modeled, including skin, eye lenses, and red bone marrow (RBM) [8,11]. Fig. 2a and 2b show the full-body and the RBM distribution of the VIP-Man model, respectively. Fig. 2c contrasts the striking anatomical differences between the two types of models. The VIP-Man model has been successfully used for Monte Carlo radiation studies of organ doses for photons, electrons, neutrons and protons [11-25].

(a) (b) (c)

Figure 2. (a) 3D rendering of the VIP-Man model; (b) Red marrow distribution. (c) A slice showing anatomical difference between the two types of models.

The International Commission on Radiological Protection has officially recognized the shift from the stylized models to tomographic models [26]. However, voxel-based models are difficult to deform and the large number of boundary crossings defined by the voxels significantly increase computing time during radiation transport in Monte Carlo simulations. It is in fact possible to combine voxel data with surface equations to design hybrid models where organ shapes are more realistically than stylized models, while maintaining the flexibility to consider anatomical variations and even organ motion. In this type of model, one can adjust the boundary of an organ to the desired shape and volume using patient-specific images and deformable image registration. However, research on hybrid models has been limited [for examples, 27-29].

Existing stylized and tomographic models that have been adopted for Monte Carlo dose calculations are 3D standing individuals which are not suitable for certain dose calculation scenarios involving the motion of certain organs or the change of posture of the body. Such scenarios include radiotherapy treatment planning of lung and prostate tumors, dose re-construction for nuclear accident, and transport if inhaled radioactive materials in the respiratory system. The ability to extend the 3D whole-body model into 4D for Monte Carlo calculations is a major breakthrough that will lead to significant improvement in radiation dosimetry, as well as other fields that depend on anatomical modeling. In this paper, a preliminary 4D computational model developed from the 3D VIP-Man voxel model is presented and its potential applications in Monte Carlo calculations are discussed.

2 MATERIAL AND METHODS

In general, a 4D anatomical model can be developed from a 3D tomographic model by varying the shape, size and location of the organs according to motion patterns that can be clinically measured. The approaches to develop a 4D model include the following general steps:

1. Feature extraction of the existing voxel model
2. Deformation the features into 4D using hypothetical equations
3. Sampling of the generated 4D model
4. Implementation of the 4D model into a Monte Carlo code

In the following section, the details of each step are described.

2.1 Feature extraction from the 3D VIP-Man model

Fig. 2a shows the internal organs of the existing 3D VIP-Man model. The visualization was rendered using visualization toolkit (VTK) (Kitware Inc., NY, 12065, USA). Each organ has a single file related with and more organs can be generated as needed. However, the original 3D VIP-Man model is based on voxels and the features of the organs are not easy to be extracted. So the first step was to convert the voxel mode into a surface model based on Non-Uniform Rational B-Splines (NURBS) surface [30]. NURBS surface is easy to deform by changing the control points and the similar approach has been done by Segars et al. [27-29]. A NURBS-based program called Rhinoceros (Robert McNeel & Associates, north Seattle, WA, 98103, USA) was used to do the conversion. Rhinoceros can create, edit, analyze, and translate NURBS curves, surfaces, and solids and also support polygon meshes. The VIP-Man organ files were changed into a format readable by Rhinoceros using a free software program called vtkEditor [31]. Once the organs were implemented into Rhinoceros, organ contours were regenerated and lofted into 3D NURBS surface as shown in Fig. 3a.

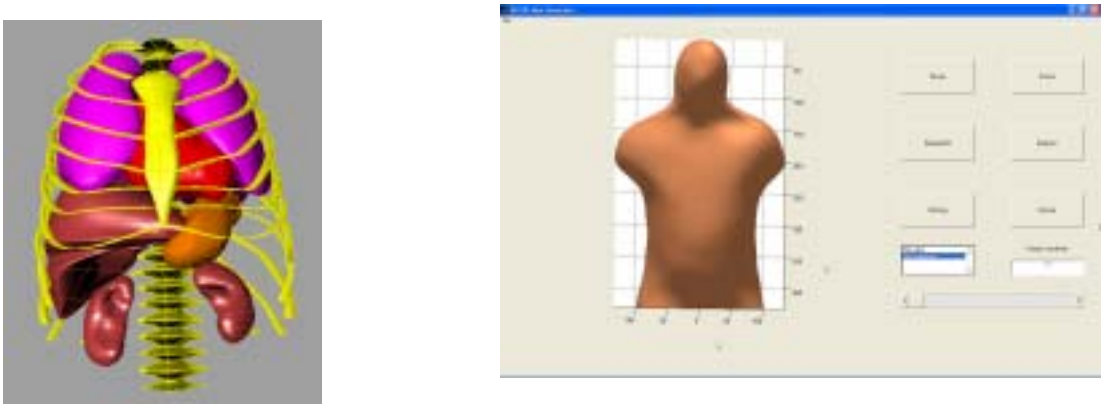

(a) (b)

Figure 3. 3D visualization of VIP-Man model: a). NURBS surface VIP-Man model. b) The graphic user interface of VIP-Man 4D program.

Note that only a portion of the organs in the VIP-Man model were used for this preliminary study. More organs will be generated using the same algorithm. After getting the NURBS surfaces for each organ, control points for each organ were obtained by exporting the files. These control points are considered as features of the 3D VIP-Man model.

2.2 Deformation of the anatomical features into 4D using hypothetical equations

The control points were saved into a matrix in Matlab (The MathWorks Inc., Natick, MA

01760, USA) and the transformation of the control points were performed by multiplying a rigid matrix as shown in Eq. 2.

$$C_{new} = S \times R \times C_{old} + T \tag{2}$$

Where C_{old} is the original matrix holding control points and C_{new} is the translated matrix holding control points. The S, R, T matrixes are 3×3 matrixes which can represent scaling, rotation and translation matrix. By selecting parameters changing with time *t* for the components of matrix S, R, and T, the control points are extended into 4D and thus the 3D VIP-Man model. In this study, respiration movement was modeled by rotating the rib cages around their intersection with the spine. The rotation angle is linear to time *t* as shown in Eq. 3.

$$\theta = \begin{cases} \Delta\theta \times t & 0 \le t < 2 \\ \frac{2}{3} \times \Delta\theta \times (5 - t) & 2 \le t < 5 \end{cases} \tag{3}$$

Where we selected Δθ to be 2.5 degree and the respiration cycle to be 5 seconds. The first 2 seconds were for inspiration and the last 3 seconds were for expiration. The sternum and skin were simulated according to the tips of ribs. The lungs were modeled referring to the fifth rib position in transverse directions and the top of the liver in longitudinal direction. For the other organs, such as liver, stomach, heart, kidneys, and one lesion in left lung, we first created a normalized motion curve as shown in Eq. 3.

$$x = \begin{cases} \frac{1}{2}\left(1 - \cos(\frac{\pi}{2} \times t)\right) & 0 \le t < 2 \\ \frac{1}{2}\left(1 - \cos(\frac{\pi}{3} \times (5 - t))\right) & 2 \le t < 5 \end{cases} \tag{4}$$

Where x is the normalized motion distance and *t* is the time. The organ motions were then modeled by multiplying different amplifying factors in x, y, z directions respectively. We used Matlab 6.5 as programming language and a NURBS toolbox [32] for Matlab was used for the developing of 4D VIP-Man program. Figure 3b shows the graphic user interface of the program. Only limited organs were integrated into the 4D model in this study. However, additional organs can be processed in the similar manner to develop a whole-body 4D VIP-Man model.

2.3 Sampling of the developed 4D model

When the 4D VIP-Man model was generated, 3D models can be sampled from the 4D model for Monte Carlo dose calculation. The sampling was done by changing the NURBS surface into organ contour and filling in the contour with different intensity number as organ ID. The control points for each organ were saved in a 3D matrix and the contour was calculated by specifying the cutting plane coordinate in the Matlab. Based on the contour points, we regenerated 2D NURBS curve as the organ contour and re-sampled 100 points on the curve. Those points are good enough to generate a polygon that is close to the original NURBS curve. Then a 2D slice (256 × 256) was initialized and each pixel was searched to determine whether the pixel was inside the

polygon or not. If the pixel was inside the polygon, an organ ID was assigned to the pixel. The sequence for searching different organs is important because the organs may overlap with each other. We searched denser organ (such as bone) later in order to override the pixel value for overlapping organs. When all the pixels and organs have been searched, the 2D slice was saved as a slice of the 3D model. A total of 70 slices were generated for each respiration phase and 8 respiration phases were sampled to represent a whole respiratory cycle: Peak exhale, early inhale, middle inhale, late inhale, peak inhale, early exhale, middle exhale, and late exhale. The image resolution is $2.1 \times 1.2 \times 6.0$ mm^3 based on this algorithm. However, more precise resolution can be generated if we increase the 2D slice size and cutting plane number.

2.4 Implementation of the 4D model into a Monte Carlo code

The sampled 3D models were implemented into a Monte Carlo code, EGS4, for dose calculation in the same way as a previous study [8]. Three dimensional simulation is done by conforming the source to the simulated lesion in the left lung for phase 8. For 4D Monte Carlo dose simulation, the 8 sets of images were implemented into the EGS4 code as one whole set image as illustrated in Fig. 4. By changing the coordinates of sampling sources according to time *t*, we calculated radiation dose in the 4D model.

The temporal resolution is 0.625 second for this study and each temporal step is set to a specific number of photon histories. The energy for the photons is 6 MeV and the irradiation geometry is anterior-posterior (AP). The lesion is a sphere with 5mm radius. The statistical uncertainty is controlled less than 1% for 1×10^7 particles. The cut off energies for electron and photon are set to 100 keV. The simulation is done on a personal computer with 2.66 GHz CPU and the simulation time is about 3 hours for each phase. All the simulation is done under Red Hat 9.0 operation system.

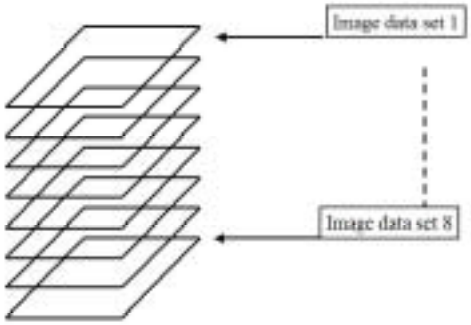

Figure 4. Implementation of the 4D model in the Monte Carlo code by piling the 8 sets of images.

3 RESULTS AND DISCUSSION

Fig. 5 (a) shows one of the 2D slices for phase 1 and the Fig. 5(b) shows 3D reconstruction based the 2D slices. The 3D reconstruction shows discontinuity for thin organ, such as ribs. The discontinuity of the 3D images is due to space resolution and can be improved when we use higher resolution for sampling.

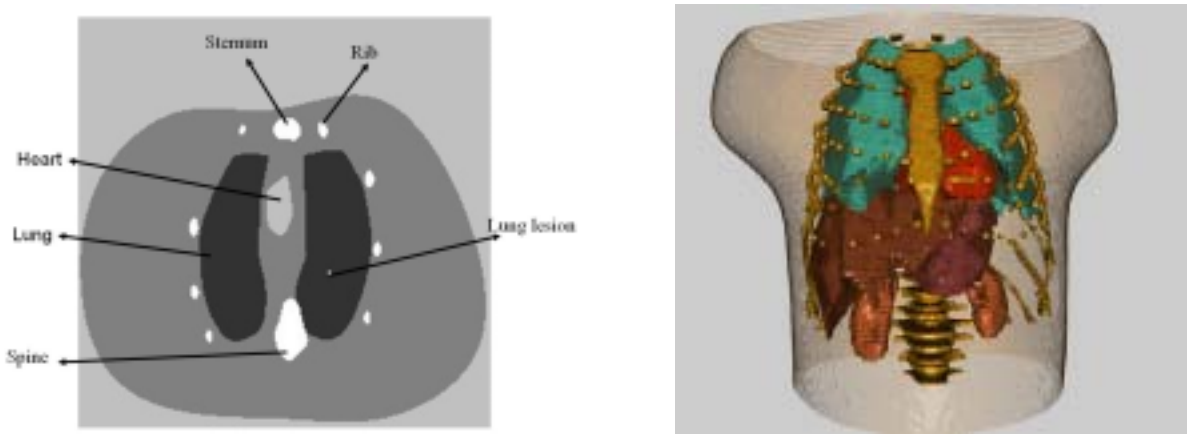

(a) (b)

Figure 5. 2D and 3D visualization: (a) 2D slice for phase 1. (b) 3D reconstruction for phase 1.

Figure 6 shows time curve for rotation angle of ribs and lung volume. The volume change agrees well with normal breathing [27].

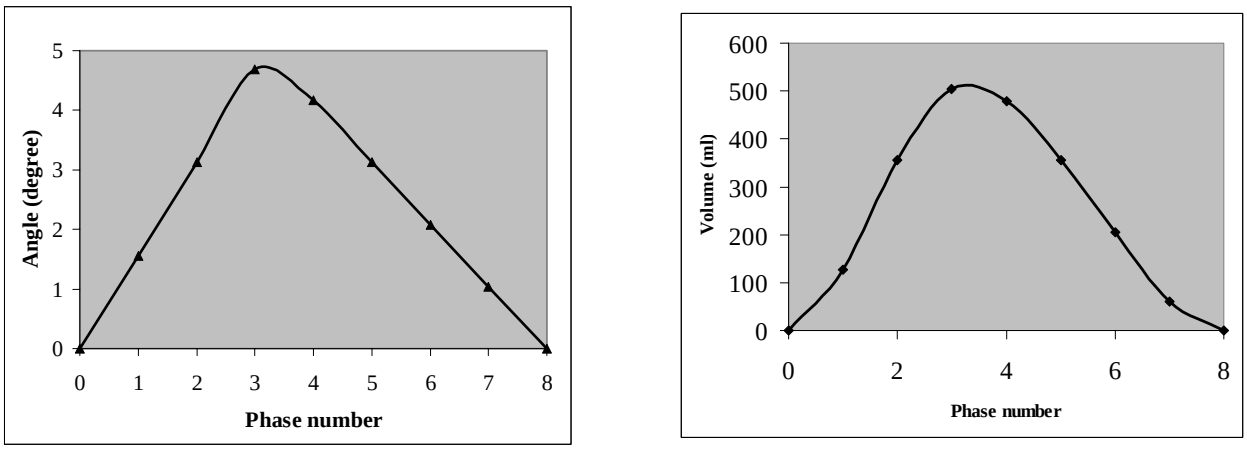

(a) (b)

Figure 6. (a) The rib rotation angle for each motion phase (The time between the phases is 0.625 second). (b) The lung volume for each motion phase.

Absorbed dose to the lung lesion was normalized to each photon and is shown in Fig. 7. The phase number corresponds to individual respiration phase. Since the photon field is conformed to the size of the lesion for the Phase 8, the change in the position of the lesion will cause dose to the lesion to vary for other phases. When the lesion moves from the Phase 8 to the Phase 3, the lesion only received 4.49% of the dose for Phase 8. Using the 4D model, the dose to the lesion for the entire respiration cycle (the straight line in Fig. 7) was determined to be about 40% of the dose for Phase 8. The dose to the lesion obtained form the 4D model differs by 2.37% from the dose to the lesion obtained from averaging doses from each of the 8 phases.

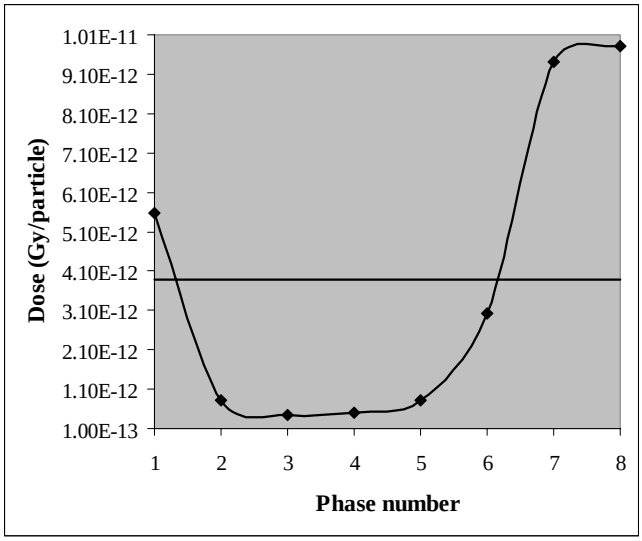

Figure 7. Normalized absorbed dose to the lung lesion for different phase of the lung motion.

4 CONCLUSIONS

A partial-body 4D VIP-Man model has been developed using the NURBS and implemented into the EGS Monte Carlo code for dose calculations. A lesion has been modeled inside the lung to calculate the change in the absorbed dose from an external photon source having the same size as the lesion. This preliminary study demonstrates that the motion of the organs can be modeled in the Monte Carlo code for more accurate dose calculations. Another potential application of this 4D model is the study for motion artifacts associated with multi-slice CT scans. In that study, the x-ray transmission through the 4D model can be simulated in a similar manner as described here.

5 REFERENCES

[1] Cristy, M. and Eckerman, K, *Specific absorbed fractions of energy at various ages from internal photons sources*, ORNL/TM-8381, V1-V7, Oak Ridge National Laboratory, Oak Ridge, TN, USA (1987).

[2] International Commission on Radiological Protection, *Conversion coefficients for use in radiological protection against external radiation*, ICRP Publication 74, Pergamon Press., Oxford, UK (1996).

[3] International Commission on Radiological Protection, Report of the Task Group on *Reference Man*, ICRP Publication 23, Pergamon Press, Oxford, UK (1975).

[4] International Commission on Radiation Units and Measurements, *Phantoms and computational models in therapy, diagnosis and protection*, ICRU Report 48, Bethesda, MD, UAS (1992).

[5] International Commission on Radiation Units and Measurements, *Measurement of dose*

equivalents from external photon and electron radiations, ICRU Report 47, Bethesda, MD, USA (1992).

[6] International Commission on Radiological Protection, *Radiation dose to patients from radiopharmaceuticals : addendum 2 to ICRP publication 53, also includes addendum 1 to ICRP publication 72*, ICRP Publication 80, Pergamon Press, Oxford, UK (1998).

[7] Caon M., "Voxel-based computational models of real human anatomy: a review," *Radiation and Environmental Biophysics*, **42 (4)**, pp.229-235 (2004).

[8] Xu XG, Chao TC, Bozkurt A., "VIP-Man: an image-based whole-body adult male model constructed from color photographs of the visible human project for multi-particle Monte Carlo calculations," *Health Phys.* **78(5)**, pp.476-486 (2000).

[9] National Library of Medicine (US) Board of Regents, *Electronic Imaging: Report of the Board of Regents*, US Department of Health and Human Services, Public Health Service, National Institutes of Health, NIH Publication 90-2197 (1990).

[10] Ackerman MJ, "Accessing the visible human project. D-lib Magazine: The Magazine of the Digital Library Forum," http://www.dlib.org/dlib/october95/10ackerman.html (1995).

[11] Xu, X. G., Chao, T.C., Bozkurt A., "VIP-Man: An image-based whole-body adult male model constructed from color photographs of the visible human project for multi-particle Monte Carlo calculations," *Health Physics*, **78(5)**, pp.476-486 (2000).

[12] Bozkurt A., Chao, T.C., Xu, X. G., "Fluence-to-Dose Conversion Coefficients from Monoenergetic Neutron Beams below 20 MeV Based on the VIP-Man Anatomical Model," *Physics in Medicine and Biology*, **45**, pp.3059-3079 (2000).

[13] Chao, T.C., Xu, X. G., "Specific absorbed fractions from the image-based VIP-Man body model and EGS4-VLSI Monte Carlo code: Internal electron emitters," *Phys. Med. Biol.*, **46**, pp.901-927 (2001).

[14] Chao, T.C., Bozkurt, A., Xu, X. G., "Conversion Coefficients Based on VIP-Man Anatomical Model and EGS4-VLSI code for Monoenergetic Photon Beams from 10 keV to 10 MeV," *Health Physics*, **81(2)**, pp.163-183 (2001).

[15] Bozkurt A., Chao, T.C., Xu, X. G., "Fluence-to-Dose Conversion Coefficients Based on The VIP-Man Anatomical Model and MCNPX Code for Monoenergetic Neutron Beams Above 20 MeV," *Health Physics*, **81(2)**, pp.184-202 (2001).

[16] Chao, T.C., Bozkurt, A., Xu, X. G., "Dose conversion coefficients for 0.1-10 MeV electrons calculated for the VIP-Man tomographic model," *Health Physics*, **81(2)**, pp.203-214 (2001).

[17] Xu, X.G., "Dose conversion coefficients for 0.1-10 MeV electrons calculated for the VIP-Man tomographic model-Response to Zankl and Petoussi-Henss," *Health Physics*, **82(2)**, pp.255-256 (2002).

18] Xu, X.G., Chao, T.C., Bozkurt, A., "A Male Radiation Worker Model Developed From Transverse Color Images Of The Visible Human Project," *Proceedings of The Fourth Visible Human Conference*, Keystone, Colorado, USA, October 17-19, 2002.

[19] Xu, X.G. and Chao, T.C., "Calculations of Specific Absorbed Fractions For GI-Tract using A Realistic Whole-Body Tomographic Model," *Cancer Biotherapy and Radiopharmaceuticals*, **18 (3)**, pp.431-436 (2003).

[20] Winslow, M., Huda, W., Xu, X.G., Chao, T.C., Shi, C.Y., Ogden, K.M., Scalzetti, E.M., "Use of the VIP-Man Model to Calculate Energy Impacted and Effective Dose for X-ray Examinations," *Health Physics*, **86(2)**, pp.174-182 (2004).

[21] Winslow, M., Xu, X.G., Huda, W., Ogden, K.M., Scalzetti, E.M., "Monte Carlo Simulations of Patient X-ray Images," *American Nuclear Society Transactions*, **90**, pp.459-460 (2004).

[22] Chao, T.C. and Xu, X.G., "S－Values Calculated from a Tomographic Head/brain Model For Brain Imaging," *Phys. Med. Biol.*, **49**, pp.4971-4984 (2004).

[23] Xu, X. G., Chao, T.C., and Bozkurt, A., "Comparison of Effective Doses from Various Monoenergetic Particle Based On the Stylized and the VIP-Man Tomographic Models," Accepted by *Rad Prot. Dosimetry* (2004).

[24] Wang B., Goldstein, M., Xu, X.G., Sahoo, N., "Adjoint Monte Carlo method for prostate external photon beam treatment planning: An application to 3-D patient anatomy," Accepted by *Phys. Med. Biol.* (2004).

[25] Bozkurt, A. and Xu, X.G., "Fluence-To-Dose Conversion Coefficients For Monoenergetic Proton Beams Based On The VIP-Man Anatomical Model," Accepted by *Rad Prot. Dosimetry* (2004).

[26] ICRP Report, http://www.icrp.org/docs/2002_Ann_Rep_52_429_03.pdf (2004).

[27] Segars, W.P., *Development and application of the new dynamic NURBS-based cardiac-torso (NCAT) phantom*, Dissertation in Biomedical Engineering, University of North Carolina: Chapel Hill, NC, USA (2001).

[28] Garrity, J.M., Segars, W.P., Knisley, S.B., Tsui, B.M.W., "Development of a dynamic model for the lung lobes and airway tree in the NCAT phantom," *IEEE Transactions on Nuclear Science*, **50(3)**, pp. 378-383 (2003).

[29] W. Paul Segars, Benjamin M. W. Tsui, Eric C. Frey, G. Allan Johnson, and Stuart S. Berr. Development of a 4D Digital Mouse Phantom for Molecular Imaging Research, Molecular Imaging and Biology, 2004.

[30] Piegl, L., "On NURBS: A Survey," *IEEE Computer Graphics and Applications*, **11**, pp. 55-71 (1991).

[31] http://www.esat.kuleuven.ac.be/~vtkedit (2004).

[32] http://www.aria.uklinux.net/nurbs.php3 (2004).